Kinematic and dynamic modeling of a multifunctional rehabilitation robot UHP

Aitziber Mancisidor[1], Asier Zubizarreta[1], Itziar Cabanes[1], Pablo Bengoa[1] and Je Hyung Jung[2]

[1]*Department of Automatics and System Engineering, University of the Basque Country (UPV/EHU), Bilbao 48013, Spain, e-mail: asier.zubizarreta@ehu.eus*
[2]*Rehabilitation Area, Health Division, TECNALIA Research and Innovation, Mikeletegi Pasealekua, 1-3 E-20009 Donostia-San Sebastian, Spain, e-mail: jehyung.jung@tecnalia.com*

Abstract. The design of a suitable controller that handles robot-human interaction is one of the critical tasks in rehabilitation robotics. For this purpose, an accurate model of the robot is required. The Universal Haptic Pantograph (UHP) is a novel upper limb rehabilitation robot that can be configured to perform arm or wrist exercises. This work is focused on the latter, solving the kinematic model by the use of the closure loop equations, while Lagrangian formulation is used to estimate the interaction force. In order to prove the effectiveness of the model, several experimental tests are carried out. Results demonstrate that the mean motion error is less than 1mm, and the estimated force error less than 10%.

Key words: Rehabilitation robots, kinematic modeling, dynamic modeling, experimental validation.

1 Introduction

Cerebrovascular diseases are the third most reason of death and the first cause of physical disability. Every year, more than 15 million strokes are diagnosed, and near 33 million people have disabilities due to the sequels of stroke [3, 13].

Hemiplegia is one of the most common stroke sequels, i.e. complete or partial paralysis of one side of the body. Currently, there is no surgical or pharmacological treatment, but according to various researches, thanks to brain plasticity, patients may recover most of their abilities by performing proper rehabilitation exercises [5, 10]. However, these treatments are time consuming and requiere constant supervision of a physiotherapist to prove effective, which increases their economic cost, and lead to the reduction of rehabilitation times.

In recent years, rehabilitation robots have been proposed as a complement to traditional physiotherapy approaches [17]. Robots emulate and replicate the motions and forces produced by a physiotherapist, executing longer, more accurate and higher frequency treatments. In addition, robots can be used as a measurement tool that quantifies forces and/or movements, with the objective of evaluating patients progress and adapting the exercises to their needs. And using a graphical interface,

a virtual reality environment can be built, so that the patient is encouraged to continue with the rehabilitation process.

The first rehabilitation robots were designed in the late eighties, and since then, many more have been proposed [1, 6]. Although there have been important advances in the area, there are still unresolved issues that need further studies, such as the design of appropriate, robust and safe control.

In the literature, several approaches are proposed to control the human-robot interaction in rehabilitation robotics: force control [14], computed torque control [9], admittance control [15], impedance control [2, 12] or algorithms using EMG signals [4, 11]. However, the implementation of these controllers requires, in most cases, a proper mathematical model of the robotic device, and the use of expensive force sensors.

In this article, kinematic and dynamic models of the Universal Haptic Pantograph (UHP) [8] are presented. The UHP is an upper limb rehabilitation robot with the ability to change its structure to perform different training exercises. This work is focused on one of the most complex modes, on the so-called Wrist mode, which is used to execute wrist training exercises. The developed models will be used to implement sensorless control approaches, with the goal of estimating the human-robot interaction force and motion during the rehabilitation exercises.

The article is organized as follows: in section II the UHP rehabilitation robot is described; in section III its kinematic and dynamic models are obtained for the Wrist mode; in section IV, to validate the models, several experimental cases are carried out; finally, the most important ideas and future work are summarized in the conclusions.

2 Universal Haptic Pantograph

The Universal Haptic Pantograph (UHP) robot is designed to execute upper limb training rehabilitation exercises after a stroke [7, 8]. One of the main advantages of the UHP is the possibility to vary its mechanical structure by using lockable/unlockable joints, allowing different types of exercises with the same robot. This way, the UHP can perform rehabilitation of the shoulder, elbow and the wrist by proper configuration of the robot.

Among the upper limb rehabilitation robots, the rehabilitation of the wrist is one of the more complex and least developed. The UHP provides a mechanical configuration that allows to perform pronation/supination, radial/unradial and flexion/extension wrist movements.

In order to allow these motions, the UHP is designed as the coupling of two subsystems. The interaction with the patient is carried out by a Pantograph structure (Fig. 1), while its actuation (i.e. the force feedback and sensing) is carried out by two perpendicular SEAs (Series Elastic Actuator). As both subsystems are connected, the torque exerted by the motors ($\boldsymbol{\tau_m}$) and the force exerted by the patient ($\mathbf{F_{Cn}}$)

are transmitted bilaterally between both subsystems in the form of force ($\mathbf{F_{Tr}}$) and motion ($\mathbf{x_{Tr}}$).

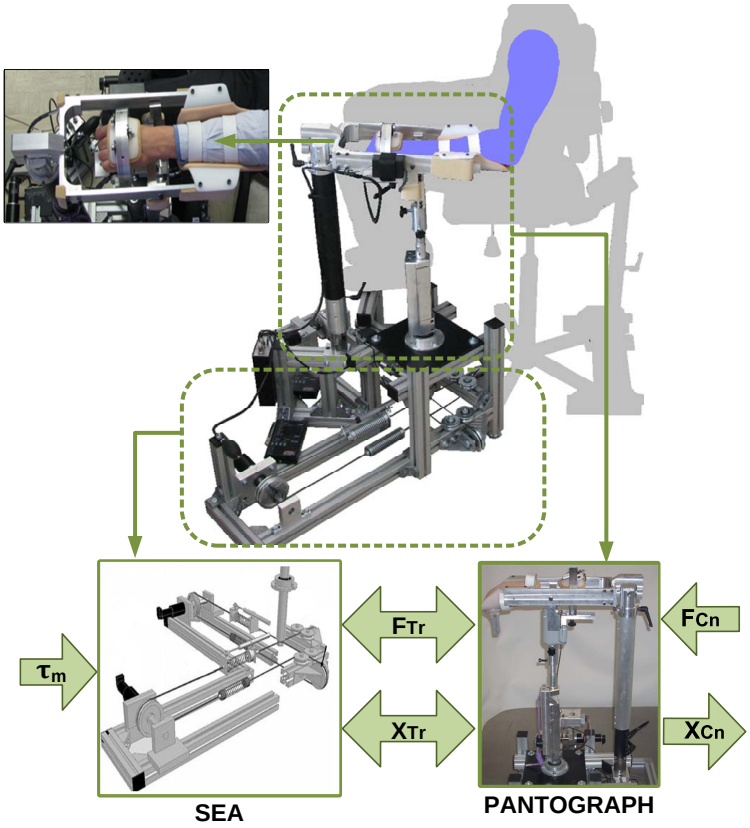

Fig. 1 Universal Haptic Pantograph (UHP)

The drive system is composed by two perpendicular SEAs with two Maxon 40 rotative motors (m_1 and m_2), four elastic springs (S_A, S_B, S_C and S_D) and a series of pulleys. The SEA subsystem is connected to the Pantograph in the transmission point ($\mathbf{P_{Tr}}$) (Fig. 2).

Force and motion transmission is carried out by using cables so that force ($\mathbf{F_{Tr}}$) and motion ($\mathbf{x_{Tr}}$) is transmitted to the Pantograph in two perpendicular directions (x and y). This way, motor m_1 and springs S_A and S_C actuate in the x direction of $\mathbf{P_{Tr}}$ (x_{Tr}), while motor m_2, S_B and S_D actuate in the y axis direction (y_{Tr}).

The Pantograph (Fig. 3) is composed by a fixed structure, three mobile bars (actuated, transverse and parallel), and five joints (spherical joint $\mathbf{P_E}$, lockable universal joint $\mathbf{P_F}$, revolute joint $\mathbf{P_G}$, lockable revolute joint $\mathbf{P_H}$ and lockable universal joint $\mathbf{P_I}$). The actuated bar is composed by three elements ($\mathbf{E_1}$, $\mathbf{E_2}$, $\mathbf{E_3}$), separated by a variable length slider and a $\mathbf{P_F}$ universal joint.

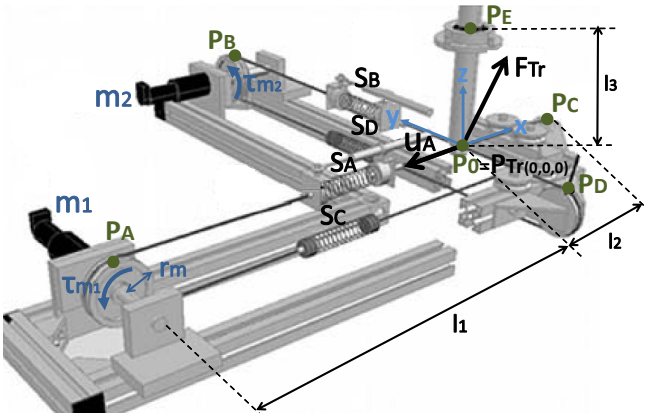

Fig. 2 Series Elastic Actuator (SEA)

In Wrist mode, joint $\mathbf{P_H}$ is partially locked and joint $\mathbf{P_I}$ is fully locked. Therefore, the parallel bar is always normal to the fixed structure, and the transverse bar ($\mathbf{E_T}$) is locked in parallel to the fixed structure, but allowing rotations along its axis $\overrightarrow{\mathbf{P_H P_G}}$ (i.e., l_{10} is constant). In order to allow actuated bar motion, the slider d_1 is used and the universal joint $\mathbf{P_F}$ is unlocked. Hence, hemispherical motions can be generated in the hand grip, conducting wrist training exercises in all possible directions.

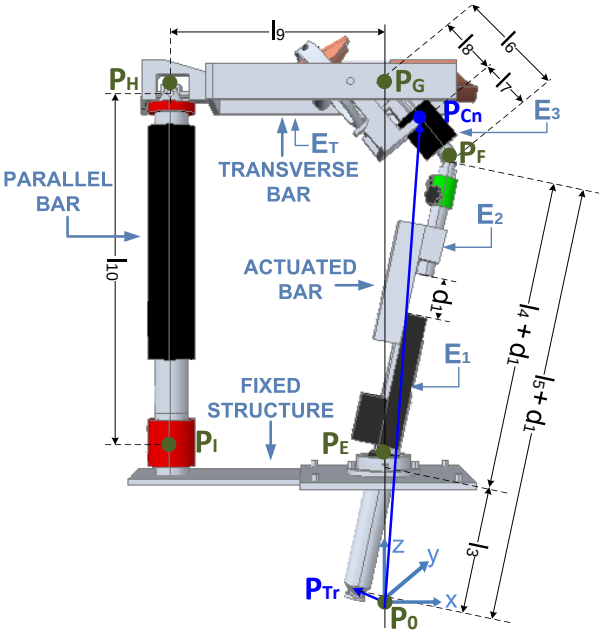

Fig. 3 Pantograph in Wrist mode

The equilibrium position of the UHP is achieved when the actuated bar is in vertical position (Fig. 3), defining the origin of the base reference frame $\mathbf{P_0}$ ($\mathbf{x_{Tr}} = \overrightarrow{\mathbf{P_0P_{Tr}}} = [0\ 0\ 0]^T$).

3 Kinematic and dynamic modeling

As mentioned previously, a proper mathematical model of the robot is required to implement the robot patient-force interaction controller. Therefore, in this section UHP kinematic and dynamic models are presented. First, in section 3.1 the drive system SEA model is obtained. Then, in section 3.2 the model of the Pantograph in Wrist mode is calculated.

3.1 The drive system SEA model

Kinematic Model of the SEA

First, the drive system kinematics is analyzed, which is composed by two perpendicular SEA systems, with one rotary actuator in each, and two sets of springs, being the upper ones sensorized by means of linear potentiometers.

Hence, the main goal of this section is to define the relationship between measurable variables, motor rotation angle ($\mathbf{q_m} = [q_{m_1}\ q_{m_1}]^T$), upper springs variable length (n_{S_A} and n_{S_B}), and output contact motion ($\mathbf{x_{Tr}} = \overrightarrow{\mathbf{P_0P_{Tr}}}$).

From Fig. 2, considering that the cables are stiff and both SEAs dimensions identical,

$$\begin{aligned} \overrightarrow{\mathbf{P_0P_{Tr}}} &= \overrightarrow{\mathbf{P_0P_A}} + \overrightarrow{\mathbf{P_AP_{Tr}}} \\ \overrightarrow{\mathbf{P_0P_{Tr}}} &= \overrightarrow{\mathbf{P_0P_B}} + \overrightarrow{\mathbf{P_BP_{Tr}}} \end{aligned} \tag{1}$$

Operating these equations,

$$\begin{aligned} \overrightarrow{\mathbf{l_A}} = \overrightarrow{\mathbf{P_AP_{Tr}}} = \overrightarrow{\mathbf{P_0P_{Tr}}} - \overrightarrow{\mathbf{P_0P_A}} = \begin{bmatrix} x_{Tr} \\ y_{Tr} \\ z_{Tr} \end{bmatrix} + \begin{bmatrix} l_1 \\ 0 \\ 0 \end{bmatrix} \\ \overrightarrow{\mathbf{l_B}} = \overrightarrow{\mathbf{P_BP_{Tr}}} = \overrightarrow{\mathbf{P_0P_{Tr}}} - \overrightarrow{\mathbf{P_0P_B}} = \begin{bmatrix} x_{Tr} \\ y_{Tr} \\ z_{Tr} \end{bmatrix} - \begin{bmatrix} 0 \\ l_1 \\ 0 \end{bmatrix} \end{aligned} \tag{2}$$

where l_1 is the distance from the equilibrium point to the position of the motor, and $\overrightarrow{\mathbf{l_i}}$ is the distance between $\mathbf{P_i}$ and the transmission point $\mathbf{P_{Tr}}$, $i = A,B,C,D$ (Fig. 2).

If each vector module is calculated, the relationship between distances l_A and l_B and $\mathbf{x_{Tr}} = [x_{Tr}\ y_{Tr}\ z_{Tr}]^T$ is obtained,

$$\begin{aligned} l_A &= \left|\overrightarrow{\mathbf{l_A}}\right| = \sqrt{(x_{Tr}+l_1)^2 + y_{Tr}^2 + z_{Tr}^2} \\ l_B &= \left|\overrightarrow{\mathbf{l_B}}\right| = \sqrt{x_{Tr}^2 + (y_{Tr}-l_1)^2 + z_{Tr}^2} \end{aligned} \tag{3}$$

On the other hand, the variable length of springs S_A and S_B (n_{S_A}, n_{S_B}) depends on distances l_A, l_B and the rotation angle of the motors (q_{m_1}, q_{m_2}),

$$\begin{aligned} n_{S_A} &= l_A + q_{m_1} r_m - l_1 \\ n_{S_B} &= l_B + q_{m_2} r_m - l_1 \end{aligned} \tag{4}$$

where r_m is the pulley radius.

Therefore, using Eqs. 3 and 4, the relationship between the motion transmission ($\mathbf{x_{Tr}}$) and the measured variables (q_{m_1}, q_{m_2}, n_{S_A}, n_{S_B}) can be calculated,

$$\begin{aligned} n_{S_A} - q_{m_1} r_m &= \sqrt{(x_{Tr}+l_1)^2 + y_{Tr}^2 + z_{Tr}^2} - l_1 \\ n_{S_B} - q_{m_2} r_m &= \sqrt{x_{Tr}^2 + (y_{Tr}-l_1)^2 + z_{Tr}^2} - l_1 \end{aligned} \tag{5}$$

As $\mathbf{x_{Tr}}$ has three variables (x_{Tr}, y_{Tr} and z_{Tr}), a third equation is required to solve the equation system. For that purpose the motion of the actuated bar is analyzed. The actuated bar presents a spherical joint $\mathbf{P_E}$ with respect to a fixed structure. Hence, the motion of $\mathbf{P_{Tr}}$ ($\mathbf{x_{Tr}}$) is constrained to the surface of a sphere of radius l_3,

$$x_{Tr}^2 + y_{Tr}^2 + (l_3 - z_{Tr})^2 = l_3^2 \tag{6}$$

Eqs. 5 and 6 define the input-output kinematic model of the SEA. However, in order to fully define the motion of the SEA subsystem, the nonsensorized lower springs deformation n_{S_C} and n_{S_D} must be calculated. For that purpose, a similar procedure as the one applied for the sensorized ones is applied,

$$\begin{aligned} l_C &= \left|\overrightarrow{\mathbf{l_C}}\right| = \left|\overrightarrow{\mathbf{P_C P_{Tr}}}\right| = \left|\overrightarrow{\mathbf{P_0 P_{Tr}}} - \overrightarrow{\mathbf{P_0 P_C}}\right| = \sqrt{(x_{Tr}-l_2)^2 + y_{Tr}^2 + z_{Tr}^2} \\ l_D &= \left|\overrightarrow{\mathbf{l_D}}\right| = \left|\overrightarrow{\mathbf{P_D P_{Tr}}}\right| = \left|\overrightarrow{\mathbf{P_0 P_{Tr}}} - \overrightarrow{\mathbf{P_0 P_D}}\right| = \sqrt{x_{Tr}^2 + (y_{Tr}+l_2)^2 + z_{Tr}^2} \end{aligned} \tag{7}$$

Hence, the variable length of the lower springs (n_{S_C}, n_{S_D}) in terms of the motors rotation angle (q_{m_1}, q_{m_2}) and the transmission motion ($\mathbf{x_{Tr}}$),

$$\begin{aligned} n_{S_C} &= l_C + q_{m_1} r_m - l_2 = \sqrt{(x_{Tr} - l_2)^2 + y_{Tr}^2 + z_{Tr}^2} + q_{m_1} r_m - l_2 \\ n_{S_D} &= l_D + q_{m_2} r_m - l_2 = \sqrt{x_{Tr}^2 + (y_{Tr} + l_2)^2 + z_{Tr}^2} + q_{m_2} r_m - l_2 \end{aligned} \tag{8}$$

Dynamic Model of the SEA

Once defined the kinematic model of the SEA, its dynamic model can be calculated. As the SEA is based on a motor-spring actuation, the exerted force will be obtained based on the spring forces that are transmitted through the cables.

The magnitude of each spring force F_{S_i} depends on its variable length n_{S_i} and its spring constant k_{S_i}, while its direction depends on the transmission motion $\mathbf{x_{Tr}}$,

$$\mathbf{F_{S_i}}(n_{S_i}, \mathbf{x_{Tr}}) = k_{S_i} n_{S_i} \mathbf{u}_i \tag{9}$$

where $\mathbf{u}_i$ is the unitary direction vector of $\mathbf{P_{Tr}P}_i$, $i = A, B, C, D$, which depends on $\mathbf{x_{Tr}}$, as calculated in section 3.1.

As the transmission point is fixed to the cables, the transmitted force vector $\mathbf{F_{Tr}}$ can be calculated by adding the forces transmitted by all cables attached to this point,

$$\mathbf{F_{Tr}} = \mathbf{F}_{S_A} + \mathbf{F}_{S_B} + \mathbf{F}_{S_C} + \mathbf{F}_{S_D} = \sum_{i=A}^{D} \mathbf{F}_{S_i} \tag{10}$$

On the other hand, the actuation torque exerted by each motor $j = 1, 2$ is calculated by using their inertia coefficient I_{m_j}, the torsional viscous friction coefficient B_{m_j}, and the Coulomb friction torque defined with coefficient F_{c_j} and β_j [16],

$$\tau_{m_j} - \tau_{S_j} = I_{m_j} \ddot{q}_{m_j} + B_{m_j} \dot{q}_{m_j} + F_{c_j} \tanh(\beta_j \dot{q}_{m_j}) \tag{11}$$

where $\tau_{S_1} = \tau_{S_{AC}}$ in motor m_1 and $\tau_{S_2} = \tau_{S_{BD}}$ in motor m_2 define the equivalent torques exerted by the springs,

$$\begin{aligned} \tau_{S_{AC}} &= \tau_{S_A} + \tau_{S_C} = \mathbf{F}_{S_A} r_m + \mathbf{F}_{S_C} r_m \\ \tau_{S_{BD}} &= \tau_{S_B} + \tau_{S_D} = \mathbf{F}_{S_B} r_m + \mathbf{F}_{S_D} r_m \end{aligned} \tag{12}$$

3.2 Pantograph model in Wrist mode

In this section the kinematic and dynamic models of the Pantograph on Wrist mode are analyzed.

Kinematic Model of the Pantograph

First, its kinematic model, that relates the motion the contact point $\mathbf{P_{Cn}}$, whose position is defined by $\mathbf{x_{Cn}} = [x_{Cn} \;\; y_{Cn} \;\; z_{Cn}]^T$, and the transmission point $\mathbf{P_{Tr}}$, whose position is defined by vector $\mathbf{x_{Tr}} = [x_{Tr} \;\; y_{Tr} \;\; z_{Tr}]^T$, is calculated based on the kinematic loop equation from Fig. 3,

$$\overrightarrow{\mathbf{P_E P_F}} + \overrightarrow{\mathbf{P_F P_G}} + \overrightarrow{\mathbf{P_G P_E}} = \mathbf{0} \tag{13}$$

Solving for $\mathbf{x_{Cn}}$,

$$\begin{bmatrix} x_{Cn} \\ y_{Cn} \\ z_{Cn} \end{bmatrix} = -\frac{(l_4 + d_1)\, l_8}{l_3 l_6} \begin{bmatrix} x_{Tr} \\ y_{Tr} \\ z_{Tr} \end{bmatrix} + \begin{bmatrix} 0 \\ 0 \\ l_3 + l_{10} + \frac{l_8 (l_4 + d_1 - l_{10})}{l_6} \end{bmatrix} \tag{14}$$

As it can be seen in Eq. 14, d_1 must be calculated to solve the equation system. As l_6 is a constant distance,

$$l_6 = \left| \overrightarrow{\mathbf{l_6}} \right| = \sqrt{\left(\frac{l_4 + d_1}{l_3} x_{Tr} \right)^2 + \left(\frac{l_4 + d_1}{l_3} y_{Tr} \right)^2 + \left(\frac{l_4 + d_1}{l_3} z_{Tr} + l_{10} - (l_4 + d_1) \right)^2} \tag{15}$$

Combining this expression with Eq. 6 and operating, d_1 can be obtained in terms of the Cartesian components of $\mathbf{x_{Tr}}$,

$$d_1 = l_{10} - l_4 + \frac{-l_{10} z_{Tr}}{l_3} \pm \sqrt{\left[\frac{l_{10} z_{Tr}}{l_3} - l_{10} \right]^2 - l_{10}^2 + l_6^2} \tag{16}$$

Hence, Eqs. 14 and 16, define the relation between the input ($\mathbf{x_{Tr}}$) and the output motion ($\mathbf{x_{Cn}}$) of the Pantograph is obtained.

The speed problem is completely defined from the calculation of the Jacobian matrices relating the output variables speed ($\dot{\mathbf{x}}_{\mathbf{Cn}}$) with the time derivative of the input variables ($\dot{\mathbf{x}}_{\mathbf{Tr}}$). Therefore, derivating Eqs. 14 and 16 with respect to time the $\mathbf{J_x}$ Jacobian can be calculated,

$$\dot{\mathbf{x}}_{\mathbf{Cn}} = \underbrace{\mathbf{J_x}}_{3x3} \dot{\mathbf{x}}_{\mathbf{Tr}} \tag{17}$$

Dynamic Model of the Pantograph

The dynamic model of the Pantograph is used to determine the relationship between the transmission force ($\mathbf{F_{Tr}}$) and the contact force vectors ($\mathbf{F_{Cn}}$) depending on the transmission motion ($\mathbf{x_{Tr}}$). For that purpose, the Lagrangian formulation is used.

In Wrist mode not all the elements of the robot move, as the fixed base and the parallel bar are locked, so their energy will be zero. In addition, the transverse

bar ($\mathbf{E_T}$) can only rotate along its axes (no potential energy) and the actuated bar elements ($\mathbf{E_1}, \mathbf{E_2}, \mathbf{E_3}$) present both rotation and translation motions due to the slider, the universal joints and the rotation of the transverse bar (Fig. 3).

Hence, kinetic ($\mathbf{K}$) and potential ($\mathbf{U}$) energies,

$$\mathbf{L} = \mathbf{K}_{E_T} + \mathbf{K}_{E_1} + \mathbf{K}_{E_2} + \mathbf{K}_{E_3} - (\mathbf{U}_{E_1} + \mathbf{U}_{E_2} + \mathbf{U}_{E_3}) \tag{18}$$

where,

$$\mathbf{K}_{E_i} = \frac{1}{2}\, m_{E_i}\, \mathbf{v}_{CM_{E_i}}^T\, \mathbf{v}_{CM_{E_i}} + \frac{1}{2}\, \omega_{CM_{E_i}}^T\, \mathbf{I}_{E_i}\, \omega_{CM_{E_i}} \tag{19}$$

$$\mathbf{U_{E_i}} = m_{E_i}\, g\, h_{CM_{E_i}} \tag{20}$$

where, m_{E_i} is the mass, $\mathbf{I}_{E_i}$ is the inertia, CM_{E_i} is the mass center and $h_{CM_{E_i}}$, $\mathbf{v}_{CM_{E_i}}$ and $\omega_{CM_{E_i}}$ are the height, linear velocity and angular velocity of the mass center of the element E_i.

Kinetic and potential energies of elements $\mathbf{E_1}$ and $\mathbf{E_2}$ are defined depending on the transmission motion ($\mathbf{x_{Tr}}$) and the ones of $\mathbf{E_3}$ and $\mathbf{E_T}$ can be obtained based on the contact motion ($\mathbf{x_{Cn}}$). The calculation of each term can be easily accomplished, and it is not detailed in this work due to space constraints. So, the Lagrangian function of the Pantograph will depend on these two sets of variables (L($\mathbf{x_{Tr}}$, $\dot{\mathbf{x}}_{\mathbf{Tr}}$, $\mathbf{x_{Cn}}$, $\dot{\mathbf{x}}_{\mathbf{Cn}}$)).

Therefore, in order to calculate the dynamic model, the Lagrangian formulation is applied to the Lagrangian defined in Eq. 18,

$$\mathbf{D_{Tr}}\ddot{\mathbf{x}}_{\mathbf{Tr}} + \mathbf{C_{Tr}}\dot{\mathbf{x}}_{\mathbf{Tr}} + \mathbf{G_{Tr}} = \frac{d}{dt}\left(\frac{\partial \mathbf{L}}{\partial \dot{\mathbf{x}}_{\mathbf{Tr}}}\right) - \frac{\partial \mathbf{L}}{\partial \mathbf{x_{Tr}}} = \sum \lambda_i \frac{\partial \Gamma(\mathbf{x_{Tr}}, \mathbf{x_{Cn}})}{\partial \mathbf{x_{Tr}}} + \mathbf{F_{Tr}} \tag{21}$$

$$\mathbf{D_{Cn}}\ddot{\mathbf{x}}_{\mathbf{Cn}} + \mathbf{C_{Cn}}\dot{\mathbf{x}}_{\mathbf{Cn}} + \mathbf{G_{Cn}} = \frac{d}{dt}\left(\frac{\partial \mathbf{L}}{\partial \dot{\mathbf{x}}_{\mathbf{Cn}}}\right) - \frac{\partial \mathbf{L}}{\partial \mathbf{x_{Cn}}} = \sum \lambda_i \frac{\partial \Gamma(\mathbf{x_{Tr}}, \mathbf{x_{Cn}})}{\partial \mathbf{x_{Cn}}} + \mathbf{F_{Cn}} \tag{22}$$

where, $\Gamma(\mathbf{x_{Tr}}, \mathbf{x_{Cn}}) = \mathbf{0}$ is the closure equation that relates the input and output variables (Eq. 13), and inertia $\mathbf{D_i}$, Coriolis $\mathbf{C_i}$ and gravity $\mathbf{G_i}$ terms can be easily calculated by grouping acceleration, velocity and gravitational terms.

If the model is to be defined in terms of $\mathbf{x_{Tr}}$, and considering that $\partial \mathbf{x_{Cn}} / \partial \mathbf{x_{Tr}} = \mathbf{J_x}$,

$$\mathbf{F_{Tr}} = \mathbf{D}\ddot{\mathbf{x}}_{\mathbf{Tr}} + \mathbf{C}\dot{\mathbf{x}}_{\mathbf{Tr}} + \mathbf{G} + \mathbf{F_E} \tag{23}$$

where,

$$\mathbf{D} = \mathbf{D_{Tr}} + \mathbf{J_x}^T \mathbf{D_{Cn}}\, \mathbf{J_x}$$

$$\mathbf{C} = \mathbf{C_{Tr}} + \mathbf{J_x}^T \mathbf{C_{Cn}}\, \mathbf{J_x} + \mathbf{J_x}^T \mathbf{D_{Cn}}\, \dot{\mathbf{J}}_{\mathbf{x}}$$

$$\mathbf{G} = \mathbf{G_{Tr}} + \mathbf{J_x}^T \mathbf{G_{Cn}}$$

$$\mathbf{F_E} = -\mathbf{J_x}^T \mathbf{F_{Cn}}$$

This equation defines the relationship between the transmission force ($\mathbf{F_{Tr}}$), the transmission motion ($\mathbf{x_{Tr}}$) and the contact force ($\mathbf{F_{Cn}}$).

4 Experimental Validation

Several experimental tests have been carried out to demonstrate the effectiveness of the calculated kinematic and dynamic models. For that purpose, the calculated models have been implemented in Matlab, and its results are compared with those obtained from the experimental tests with the UHP prototype.

In order to perform the experimental validation data captured from the UHP robot is used: both motors encoders that measure the motors rotation angle ($\mathbf{q_m}$) and the linear-potentiometers that measure the variable lengths of springs S_A and S_B (n_{S_A}, n_{S_B}). In addition, a force sensor has been integrated to measure contact force ($\mathbf{F_{Cn}}$) and a 3 axis inclinometer has been attached to the Pantograph, so that the x and y inclination angle can be measured, and the x_{Tr} and y_{Tr} variables are estimated easily.

Parameters of the UHP elements have been experimentally identified, while the motor-pulley parameters have been identified using the Grey-box procedure [16]. Real prototype parameters are summarized in Table 1 (The inertia tensors are defined as centroidal, hence, only diagonal components are detailed).

Table 1 Parameters of the UHP prototype.

Parameter	Value	Parameter	Value
l_1	$0.575m$	r_{p_1}	$0.047m$
l_2	$0.15m$	r_{p_2}	$0.0325m$
l_3	$0.18m$	I_{m_1}	$0.003615Ns^2/rad$
l_4	$0.46m$	I_{m_2}	$0.002742Ns^2/rad$
l_5	$0.64m$	B_{m_1}	$1.02 \cdot 10^{-7}Ns/rad$
l_6	$0.202m$	B_{m_2}	$5.27 \cdot 10^{-9}Ns/rad$
l_7	$0.12m$	F_{c_1}	$0.840395Nm$
l_8	$0.268m$	F_{c_2}	$0.731213Nm$
l_9	$0.268m$	β_1	4223.98
l_{10}	$0.662m$	β_2	4318.25
		k_{S_i}	$4000N/m$
m_{E_1}	$0.882kg$	I_{E_1}	$[13.5\ \ 0.49\ 13.4\ ]\ 10^{-3}kg\ m^2$
m_{E_2}	$1.25kg$	I_{E_2}	$[\ 9.7\ \ 0.59\ \ 9.51]\ 10^{-3}kg\ m^2$
m_{E_3}	$1.23kg$	I_{E_3}	$[\ 4.9\ \ 1.96\ \ 3.61]\ 10^{-3}kg\ m^2$
m_{E_T}	$1.55kg$	I_{E_T}	$[\ 40\ \ \ 13.5\ \ \ 28\ ]\ 10^{-3}kg\ m^2$

Three tests have been carried out to validate the models. First, the UHP kinematic model in Wrist mode is validated. For this purpose, motors are induced to perform a sinusoidal motion with 5s period and no contact force is applied. Motor rotation angles ($\mathbf{q_m}$), variable length of the upper springs (n_{S_A}, n_{S_B}) and actuated bar angles are measured and used to estimate the contact motion ($\mathbf{x_{Cn}}$).

In Fig. 4, the real and estimated values of $\mathbf{x_{Cn}}$ x and y componentes are observed. As it can be seen, the mean error is smaller than one millimeter and the maximum error is 6mm.

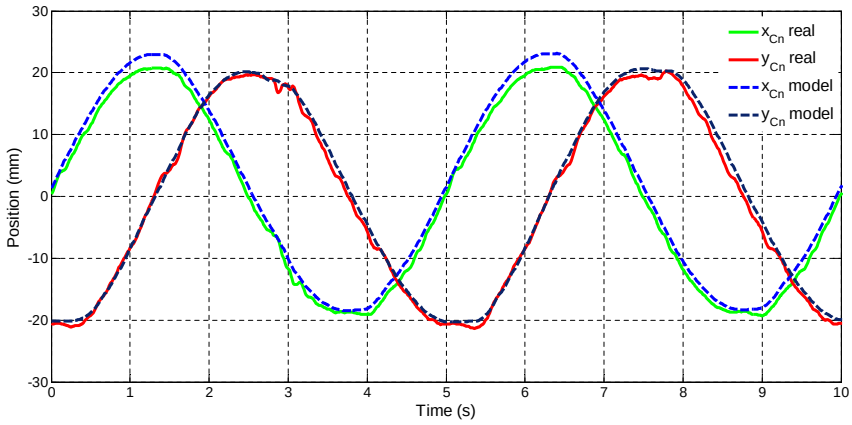

Fig. 4 Kinematic model validation test results.

The second test is used to validate the dynamic model of the drive system SEA. As forces of the SEA are related to the spring motion, the test is based on the estimation of the spring measurements and forces. For this test, the Pantograph is locked in the equilibrium position ($\mathbf{x_{Tr}} = [0\ 0\ 0]^T$) and the motors execute a sinusoidal motion with 5s period. In this case, motors torques ($\boldsymbol{\tau_m}$) and rotation angles ($\mathbf{q_m}$) and variable length of the upper springs (n_{S_A}, n_{S_B}) are measured, along with the actuated bar orientation using the inclinometer.

Based on the inclinometer data, the real $\mathbf{x_{Tr}}$ is obtained. Combining it with the measured motor position $\mathbf{q_m}$ and torque $\boldsymbol{\tau_m}$, the spring force $\mathbf{F_{Si}}$ is estimated, and using the spring constant, the variable length of the springs S_A and S_B (n_{S_A}, n_{S_B}) is calculated.

In Fig. 5, the real and estimated values of n_{S_A} and n_{S_B} are observed. In this case, the mean error is half millimeter and the maximum error is smaller than 3 mm.

In the final test, the dynamic model of the UHP robot in Wrist mode is validated. In order to achieve this, the UHP will execute a trajectory, while the user exerts external force. In this case, motor rotation angles ($\mathbf{q_m}$), variable length of the upper springs (n_{S_A}, n_{S_B}), actuated bar angles and the contact force ($\mathbf{F_{Cn}}$) are measured.

Using these measurements the transmission force ($\mathbf{F_{Tr}}$) is calculated based on the dynamic model of SEA, validated in the previous section. In addition, the transmission force is also estimated by using the contact force measurement and the dynamic model of the Pantograph on the Wrist mode. The latter is considered to be the more accurate.

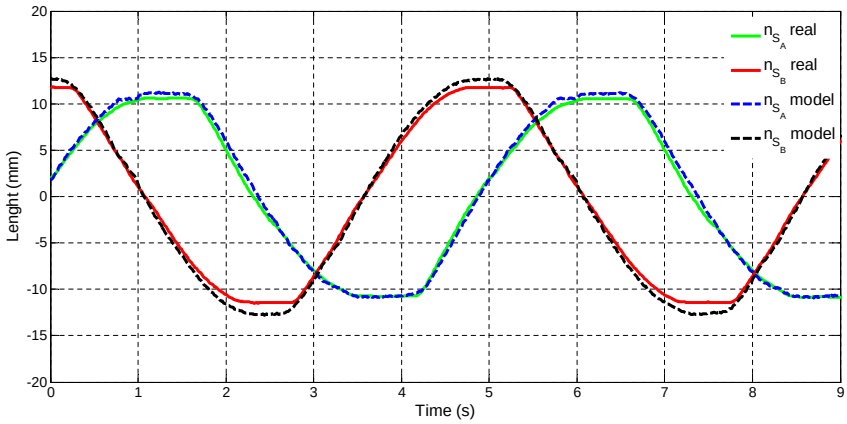

Fig. 5 Drive systems dynamic model validation test results.

In Fig. 6, the values of $\mathbf{F_{Tr}}$ obtained with the dynamic model of the SEA and with the dynamic model of the Pantograph are observed. As it can be seen, the mean error is 5N and the error is always less than the 10%.

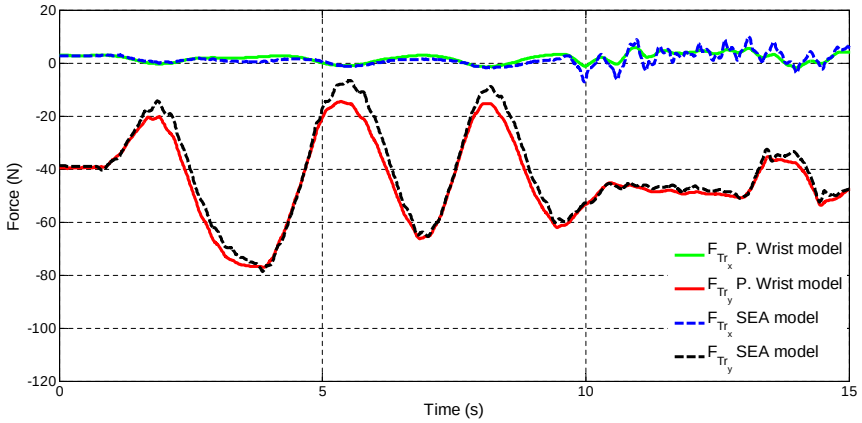

Fig. 6 UHP dynamic model validation test results.

5 Conclusions

In this work kinematic and dynamic models of a multifunctional rehabilitation robot UHP (Universal Haptic Pantograph) are presented. The UHP provides various func-

tionality modes that provide different rehabilitation exercises. This work focuses on the Wrist mode.

The UHP robot modeling is divided in two parts: the drive system, which is based on a Serial Elastic Actuator system, and a Pantograph. To solve the kinematic model, the closure equations are used, while Lagrangian formulation is used to calculate the dynamic model of the robot.

To verify the models, a set of experimental tests have been carried out. Results show that the model works properly in all relevant scenarios. The motion mean error in the contact point ($\mathbf{P_{Cn}}$) is one millimeter while the transmission force ($\mathbf{F_{Tr}}$) error is smaller than the 10%.

The calculated kinematic and dynamic model are critical to perform proper control of the robot-patient interaction. The proposed models will be used to estimate the force and motion of this interaction without the direct measurement of the contact force, hence, reducing the economical cost of the robot.

Acknowledgements This work was supported in part by the Basque Country Governments (GV/EJ) under grant PRE-2014-1-152, UPV/EHU's UFI11/25 project, Spanish Ministry of Economy and Competitiveness' MINECO & FEDER inside the DPI-2012-328822 project, Spanish Ministry of Economy and Competitiveness BES-2013-066142 grant, Euskampus, FIK and Spanish Ministry of Science and Innovation PDI-020100- 2009-21 project.

References

1. Babaiasl, M., Mahdioun, S.H., Jaryani, P., Yazdani, M.: A review of technological and clinical aspects of robot-aided rehabilitation of upper-extremity after stroke. Disability and Rehabilitation: Assistive Technology pp. 1–18 (2015). DOI 10.3109/17483107.2014.1002539
2. Carignan, C., Tang, J., Roderick, S.: Development of an exoskeleton haptic interface for virtual task training. In: 2009 IEEE/RSJ International Conference on Intelligent Robots and Systems, IROS 2009, pp. 3697–3702. IEEE/RSJ, Louis, USA (2009). DOI 10.1109/IROS.2009.5354834
3. Corbyn, Z.: A growing global burden. Nature **510**(S3), 5–6 (2014)
4. Gopura, R.A.R.C., Kiguchi, K., Li, Y.: SUEFUL-7: A 7DOF upper-limb exoskeleton robot with muscle-model-oriented EMG-based control. In: International Conference on Intelligent Robots and Systems, pp. 1126–1131. Ieee (2009). DOI 10.1109/IROS.2009.5353935. URL http://ieeexplore.ieee.org/lpdocs/epic03/wrapper.htm?arnumber=5353935
5. Harwin, W.S., Patton, J.L., Edgerton, V.R.: Challenges and opportunities for robot-mediated neurorehabilitation. Proceedings of the IEEE **94**(9), 1717–1726 (2006). DOI 10.1109/JPROC.2006.880671
6. Maciejasz, P., Eschweiler, J., Gerlach-Hahn, K., Jansen-Troy, A., Leonhardt, S.: A survey on robotic devices for upper limb rehabilitation. Journal of neuroengineering and rehabilitation **11**(1), 3 (2014). DOI 10.1186/1743-0003-11-3
7. Oblak, J., Matjačić, Z.: Design of a series visco-elastic actuator for multi-purpose rehabilitation haptic device. Journal of neuroengineering and rehabilitation **8**(January), 3 (2011). DOI 10.1186/1743-0003-8-3
8. Perry, J.C., Oblak, J., Jung, J.H., Cikajlo, I., Veneman, J.F., Goljar, N., Bizoviar, N., Matjai, Z., Keller, T.: Variable structure pantograph mechanism with spring suspension system for comprehensive upper-limb haptic movement training. The Journal of Rehabilitation Research and Development **48**(4), 317 (2011). DOI 10.1682/JRRD.2010.03.0043

9. Rahman, M.H., Ouimet, T.K., Saad, M., Kenné, J.P.: Development and Control of a Wearable Robot for Rehabilitation of Elbow and Shoulder Joint Movements. In: Conference on IEEE Industrial Electronics Society, pp. 1506–1511. IEEE (2010). DOI 10.1109/IECON.2010.5675459
10. Sawaki, L.: Use-dependent plasticity of the human motor cortex in health and disease. IEEE Engineering in Medicine and Biology Magazine **24**(1), 36–39 (2005). DOI 10.1109/MEMB.2005.1384098
11. Song, Z., Zhang, S., Gao, B.: Implementation of Resistance Training Using an Upper-Limb Exoskeleton Rehabilitation Device for Elbow Joint. Journal of Medical and Biological Engineering **34**(2), 188–196 (2013)
12. Stienen, A.H.A., Hekman, E.E.G., Ter Braak, H., Aalsma, A.M.M., Van Der Helm, F.C.T., Van Der Kooij, H.: Design of a rotational hydro-elastic actuator for an active upper-extremity rehabilitation exoskeleton. In: Proceedings of the 2nd Biennial IEEE/RAS-EMBS International Conference on Biomedical Robotics and Biomechatronics, BioRob 2008, pp. 881–888. IEEE, Scottsdale, AZ, USA (2008). DOI 10.1109/BIOROB.2008.4762873
13. Thrift, A.G., Cadilhac, D.A., Thayabaranathan, T., Howard, G., Howard, V.J., Rothwell, P.M., Donnan, G.A.: Global stroke statistics. International Journal of Stroke **9**(January), 6–18 (2014). DOI 10.1111/ijs.12245
14. Vertechy, R., Frisoli, A., Dettori, A., Solazzi, M., Bergamasco, M.: Development of a new exoskeleton for upper limb rehabilitation. In: IEEE International Conference on Rehabilitation Robotics, ICORR 2009, pp. 188–193. IEEE, Kyoto International Conference Center, Japan (2009). DOI 10.1109/ICORR.2009.5209502
15. Wen, Y., Rosen, J., Li, X.: PID admittance control for an upper limb exoskeleton. In: Proceedings of the 2011 American Control Conference, pp. 1124–1129. Ieee, O'Farrell Street, San Francisco, CA, USA (2011). DOI 10.1109/ACC.2011.5991147
16. Wernholt, E.: Nonlinear identification of a physically parameterized robot model. In: SYSID, pp. 143–148. Newcastle, Australia (2006). DOI 10.3182/20060329-3-AU-2901.00016
17. Zhou, S.H., Fong, J., Crocher, V., Tan, Y., Oetomo, D., Mareels, I.: Learning control in robot-assisted rehabilitation of motor skills a review. Journal of Control and Decision **7706**(March), 1–25 (2016). DOI 10.1080/23307706.2015.1129295